Regular article

Ping Zhang, Wenhui Yi*, Hao Xu, Chao Gao, Jin Hou, Weiqiu Jin, Yue Lei and Xun Hou

Supramolecular interactions of poly[(9,9-dioctylfluorenyl-2,7-diyl)-co-thiophene] with single-walled carbon nanotubes

https://doi.org/10.1515/ntrev-2018-0041
Received April 30, 2018; accepted September 20, 2018; previously published online October 23, 2018

Abstract: Efficient selective extraction of semiconducting single-walled carbon nanotubes (s-SWCNTs) from as-synthesized SWCNTs is essential for their electronic and photovoltaic applications. In this study, we used a relatively simple copolymer backbone structure of poly[(9,9-dioctylfluorenyl-2,7-diyl)-co-thiophene] (PFT) for the selective extraction of s-SWCNTs from HiPCO SWCNTs. The absorption and Raman spectroscopies indicated that the PFT-sorted s-SWCNTs had high purity which was far beyond the sensitivity of the spectrometers. Photoluminescence excitation spectroscopy showed that PFT mainly extracted the chiralities of (n,m) = (9,5), (8,6), (7,5), and (10,5) s-SWCNTs with the ratios of about 53.1%, 24.8%, 11.5%, and 10.5%, respectively. Both steady-state and transient optical spectroscopies suggested that there was a strong interaction between PFT and s-SWCNTs. Molecular dynamics simulation results agreed well with the experimental data. Additionally, the photoinduced energy transfer behavior of the PFT-wrapped s-SWCNT resultant hybrid was assessed. This work indicated that the prepared PFT-wrapped s-SWCNT hybrid material was attractive for organic photovoltaic devices.

***Corresponding author: Wenhui Yi,** Key Laboratory for Information Photonic Technology of ShaanXi Province, School of Information and Electronics Engineering and Key Laboratory for Physical Electronics and Devices of the Ministry of Education, Xi'an Jiaotong University, Xi'an 710049, China, e-mail: yiwenhui@mail.xjtu.edu.cn
Ping Zhang, Hao Xu, Weiqiu Jin, Yue Lei and Xun Hou: Key Laboratory for Information Photonic Technology of ShaanXi Province, School of Information and Electronics Engineering and Key Laboratory for Physical Electronics and Devices of the Ministry of Education, Xi'an Jiaotong University, Xi'an 710049, China
Chao Gao: State Key Laboratory of Fluorine and Nitrogen Chemicals, Center for Optic-Electronic Materials, Xi'an Modern Chemistry Research Institute, Xi'an 710065, China
Jin Hou: Department of Pharmacology, School of Basic Medical Sciences, Xi'an Medical University, Xi'an 710021, China

Keywords: conjugated polymer; energy transfer; photophysical properties; semiconducting single-walled carbon nanotubes.

1 Introduction

Single-walled carbon nanotubes (SWCNTs) have been expected to be a promising candidate for both microelectronics and optoelectronics application due to their excellent optical, electronic, and mechanical properties [1]. However, as-synthesized SWCNTs are mixtures of metallic SWCNTs (m-SWCNTs) and semiconducting SWCNTs (s-SWCNTs), which hinders their practical uses in high-performance electronics and photoelectricity [2]. Fortunately, many post-synthetic sorting methods have been well developed to eliminate such barrier, including density gradient ultracentrifugation [3], DNA molecule wrapping [4], and conjugated polymer wrapping [5]. Among these methods, sorting s-SWCNTs using conjugated polymer wrapping is becoming increasingly attractive for its high selectivity, high yield, and easy implementation [5–10]. In addition, due to the involvement of noncovalent functionalization, the electronic structure of SWCNTs is not disrupted during the separation process. Moreover, the resultant s-SWCNTs/polymer composite can be directly employed for some certain applications, such as fabrication of active layers in solar cells. The hybrid form avoids the additional post-processing needs, which make the approach commercially scalable. It has been reported that using polymer-sorted highly purified s-SWCNTs as a part of an active layer can greatly improve the device performance of solar cells [11–13].

In recent years, a number of conjugated polymers, including polyfluorenes [5, 14, 15], polythiophenes [10, 16], polycarbazoles [17, 18], and their copolymers [9, 19–21], have been used for sorting s-SWCNTs by wrapping around the nanotube through π-π interactions. Among them, the copolymers of fluorene and thiophene are interesting classes of materials due to their excellent stability and

wide electronic tunability via side-chain modifications [22]. Recently, Liu et al. [23] and Qian et al. [24] reported a 9,9-dioctylfluorene-co-bithlophene copolymer for selective separation of large-diameter s-SWCNTs. Using poly[2,7-(9,9-dioctylfluorene)-alt-4,7-bis(thiophen-2-yl) benzo-2,1,3-thiadiazole] wrapping arc-discharge SWCNTs, Xu et al. obtained high-purity s-SWCNT inks [25].

A large body of literature suggests that the purity, selectivity, and yield of s-SWCNTs wrapped by conjugated polymers are highly dependent on the polymer molecule structure, such as side chains or skeletons. In other words, the different molecular structures lead to different interactions with SWCNTs. Hence, more new conjugated polymers need to be explored for sorting of s-SWCNTs. Although a large number of conjugated polymers on the basis of copolymers of the fluorene and thiophene structure have been examined for enriching s-SWCNTs, the relatively simple copolymer backbone structure of poly[(9,9-dioctylfluorenyl-2,7-diyl)-co-thiophene] (PFT) has not been reported by far. Furthermore, compared with other polymers, such as poly(9,9-di-n-octylfluorenyl-2,7-diyl) (PFO), PFT has stronger electron donating ability [26]. Hence, PFT-wrapped s-SWCNTs are a potential material for photovoltaic applications.

In this study, PFT-conjugated polymers were prepared and employed to separate s-SWCNTs from HiPCO SWCNT mixtures. Ultraviolet-visible-near-infrared (UV-vis-NIR) spectroscopy and Raman spectroscopy were performed to confirm that m-SWCNTs were significantly removed from the mixtures and highly purified PFT-wrapped s-SWCNTs were successfully obtained. The photoluminescence-excitation (PLE) maps were carried out to investigate the chiralities of the sorted SWCNTs. The photophysical properties of PFT-wrapped s-SWCNTs and pure PFT were investigated by steady-state and transient optical spectroscopies. In addition, the dynamical behavior of luminescence from PFT-wrapped s-SWCNTs was studied by a rate equation model. Finally, molecular dynamics (MD) simulations were carried out so as to explain the chosen interactions between PFT and SWCNTs of different chiralities. This research may help to better understand the energy transfer process in the polymer-wrapped s-SWCNTs mixture as well as the development of photovoltaic devices.

2 Experimental section

2.1 Materials and instrument

HiPCO SWCNT powders were produced via the high-pressure disintegration of carbon monoxide, which was supplied by NanoIntegris Technologies, Inc. (Quebec, Canada). The ratio of s-SWCNTs to m-SWCNTs in the mixture of SWCNTs synthesized by such a method was 2:1. The copolymer PFT synthesized by the Suzuki coupling reaction with reference to the procedure reported in a previous publication (Scheme 1) [22] was obtained from Xi'an Modern Chemistry Research Institute (Xi'an, China). All the other solvents and reagents were obtained from profit-making suppliers and used as received.

Centrifugation was carried out by a Lu xiangyi TG16-WS centrifugator (Lu Xiangyi, Shanghai, China). The UV-vis-NIR absorption measurements were performed with a UV-2600 spectrophotometer (SHIMADZU, Columbia, SC, USA). The Raman spectra analysis was completed with a confocal Raman microscope (HR 800; Horiba Jobin Yvon, LabRAM HR Evolution; HORIBA Scientific, Paris, France) equipped with 633 nm lasers, and the peak positions were finely adjusted to be in line with the Si line at 521 cm^{-1}. The PLE spectra of near-infrared fluorescence were obtained with an FLS980 spectrometer (Edinburgh Instruments Ltd., Edinburgh, UK) at wavelength intervals of 2 and 5 nm for emission and excitation, respectively. The transient fluorescence decay of PFT-wrapped SWCNT solutions was investigated with a time-resolved fluorescence system in nanosecond timescale.

2.2 General procedures for selective extraction of s-SWCNTs with PFT in toluene

SWCNT powders were first scattered among dissolvents at the 4 mg of SWCNTs:10 mg of PFT:20 ml of toluene ratio. The solution was homogenized for 1 h via a bath-type sonicator. Then, 1-h vigorous sonication (200 W) by tip-sonication was performed. Subsequently, the resulted solution was centrifuged for 1 h at a speed of 12,000 rpm to remove sediments. The upper 80% of supernatant (PFT/s-SWCNTs) was collected and applied for further characterization.

Scheme 1: Structure and synthetic scheme of PFT.

For comparison, 1 mg of pristine SWCNTs was dispersed in 50 ml PFT toluene solution (PFT/p-SWCNTs) by multiple 1-h-tip-sonication treatments but without centrifugal treatment. In order to prevent aggregation and bundling of SWCNTs, the PFT/p-SWCNTs solution was bath-sonicated until immediately before use for characterization. We also dispersed SWCNTs in 2% sodium dodecyl sulfate (SDS) water solution and prepared the SDS/SWCNTs sample.

2.3 MD simulations

The Materials Studio software package was employed to simulate the selective interaction between PFT and SWCNTs with different chiralities. MD simulation was performed by the Forcite module, applying the COMPASSII classical force field. The initial structures for MD simulation were built up with undefined boundary conditions. The nanotubes and polymers were not fixed. Among the whole models, 10 repeating groups were applied to form the PFT polymers. The lengths of all the SWCNTs were kept equal to integer number of repeat units, and the values were limited to around 28 nm. Besides, hydrogen atoms were added at the ends of the SWCNTs for avoiding the unsaturated boundary effect. All the simulations were performed in a vacuum. In order to make the system balanced, the following consequent procedure was performed: first, simulated annealing of 500 ps with 10 heating cycles was employed to produce energy-desirable constructions for the original constructions. Here, the initial temperature of 300 K, the mid-cycle temperature of 800 K, and the constant number of molecules, constant volume, constant temperature (NVT) ensemble with the Nose thermostat were applied. Then, the lowest energy construction was selected for every PFT-SWCNT. Subsequently, 500 ps NVT simulation with the Berendsen thermostat was performed to achieve further equilibration. Finally, 200 ps constant number of molecules, constant volume, constant energy simulation was carried out so as to end the equilibrated construction. Here, when the fluctuations of non-bond energy and temperature were less than 5%, the system was considered to be in equilibrium. Unless otherwise mentioned, the time step for the whole simulations is 1 fs.

3 Results and discussions

3.1 UV-vis-NIR, Raman, and PLE characterizations

Optical absorbance studies revealed that PFT tended to be useful for the dispersion of SWCNTs. Figure 1A shows the UV-vis-NIR absorption spectra of the samples PFT/s-SWCNTs and SDS/SWCNTs. Here, SDS/SWCNTs were employed for comparison. Remarkably, the SDS/SWCNTs sample had stronger absorption peaks in the metallic M_{11} band (480–620 nm). But no obvious absorption peak in the metallic M_{11} band was observed in the absorption spectrum of the PFT/s-SWCNTs sample. In addition, compared to SDS/SWCNTs, PFT/s-SWCNTs generated well-resolved and strong signals in the S_{11} and S_{22} regions.

It is well known that the radial breathing modes (RBM) and the intense graphitic (G) band can be applied to ensure the chirality, diameter, and electronic properties.

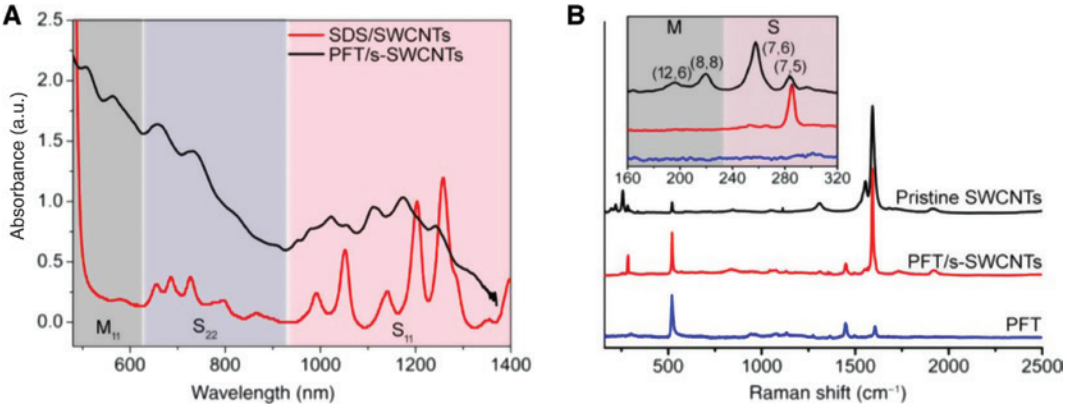

Figure 1: UV-vis-NIR absorption and Raman spectra. (A) UV-vis-NIR absorption spectrum for the PFT/s-SWCNTs (red) sample dispersed in toluene. Corresponding spectrum for the SDS-dispersed-pristine SWCNTs sample (SDS/SWCNTs) provided for reference. (B) Raman spectrum of PFT/s-SWCNTs (633 nm excitation). Spectra for the pristine SWCNTs and pure PFT are also provided for reference. The corresponding RBM regions are depicted in the insets. Note: for the insets, the box labeled "M" denotes the spectral region at which signals from m-SWCNTs are observed (160–220 cm^{-1}), while the box labeled "S" denotes the region corresponding to s-SWCNTs (230–320 cm^{-1}).

Figure 1B displays that the Raman spectra excited at 633 nm of the drop-cast of the PFT/s-SWCNTs sample, along with those of pure PFT and pristine SWCNTs for comparison. In HiPCO SWCNTs at 633 nm excitation wavelength, the RBM bands at about 160–220 cm^{-1} were attributed to m-SWCNTs, while s-SWCNTs give rise to signals within the scope of 230–320 cm^{-1} [27]. Clearly, both m-SWCNT and s-SWCNT peaks appeared in the pristine SWCNTs. But although the RBM band was magnified 10 times within the scope of 160–220 cm^{-1}, no m-SWCNT peak was present in the PFT/s-SWCNTs sample, indicating that the purity of s-SWCNTs was far beyond the sensitivity of the spectrometers. Thus, according to the UV-vis-NIR absorption and Raman spectra estimation, the purity of s-SWCNTs should be above 99% [28]. The peaks in the Raman spectra RBM region (Figure 1B) were assigned in accordance with the earlier research studies [29]. The peaks at 195 and 219 cm^{-1} were assigned to two metallic tubes of (12,6)-SWCNTs and (8,8)-SWCNTs. And the assignments of peaks at 257 and 282 cm^{-1} were subject to the semiconducting tubes of (7,6)-SWCNTs and (7,5)-SWCNTs, respectively. It was noteworthy that the peak at 257 cm^{-1} in the pristine SWCNTs sample was stronger than the peak at 282 cm^{-1}, suggesting that the pristine SWCNTs enriched (7,6)-SWCNTs rather than (7,5)-SWCNTs. However, the peak at 257 cm^{-1} in the PFT/s-SWCNTs sample almost disappeared, but the peak at 282 cm^{-1} was stronger, indicating that the PFT selectively extracted (7,5)-SWCNTs rather than (7,6)-SWCNTs.

The Raman G band included the G^- band (1520–1560 cm^{-1}) and G^+ band (around 1590 cm^{-1}), indicating the content of m-SWCNTs and s-SWCNTs, respectively [29]. Compared to pristine SWCNTs, the narrow and weaker G^- band feature further confirmed a significantly low content of metallic tubes in the PFT/s-SWCNTs sample.

The Raman D-bands at 1310 cm^{-1}, which are defectively sensitive for SWCNTs, were almost invisible in the PFT/s-SWCNTs sample, which meant that there were no observable defects brought into the nanotubes during the isolation processes.

PLE spectroscopy is the effective helper for the determination of chirality indices of individually solubilized SWCNTs [30, 31]. Figure 2 shows the PLE mappings of the PFT/s-SWCNTs and PFT/p-SWCNTs samples. Here, the PFT/p-SWCNTs sample for comparison was used, because the PFT/p-SWCNTs sample was unable to selectively sort s-SWCNTs from HiPCO SWCNTs but had better dispersivity than the SDS/SWCNTs sample. Among these spectra, the chiralities of SWCNTs were assigned according to previously published data [30, 32]. In the PLE mappings of PFT/p-SWCNTs, many (n,m)-SWCNTs were observed, such as (6,5)-, (7,5)-, (7,6)-,(8,4)-, (8,6)-, (8,7)-, (9,4)-, (9,5)-, (10,3)-, (10,5)-, and (11,3)-SWCNTs. Among them, fluorescence intensity from (9, 5)-SWCNTs was most evident. After sorted by PFT, the underlying background and SWCNTs species were greatly reduced. But the fluorescence intensity from (9, 5)-SWCNTs remained strongest (Figure 2B). The PLE mappings suggested that the PFT mainly extracted the chiralities of the s-SWCNTs with (n,m) = (9,5), (8,6), (7,5), and (10,5). We used the method described in [33] to calculate the ratio of the sorted (n,m)-SWCNTs, and the results are recorded in Table 1. The amount ratios of the extracted s-SWCNT chiralities of (9,5), (8,6), (7,5), and (10,5) were 53.1%, 24.8%, 11.5%, and 10.5%, respectively.

3.2 Steady-state and transient photophysical properties

The steady-state photophysical properties of PFT, PFT/s-SWCNTs, and PFT/p-SWCNTs were typical of UV-vis-absorption spectroscopy in a toluene solution (Figure 3A).

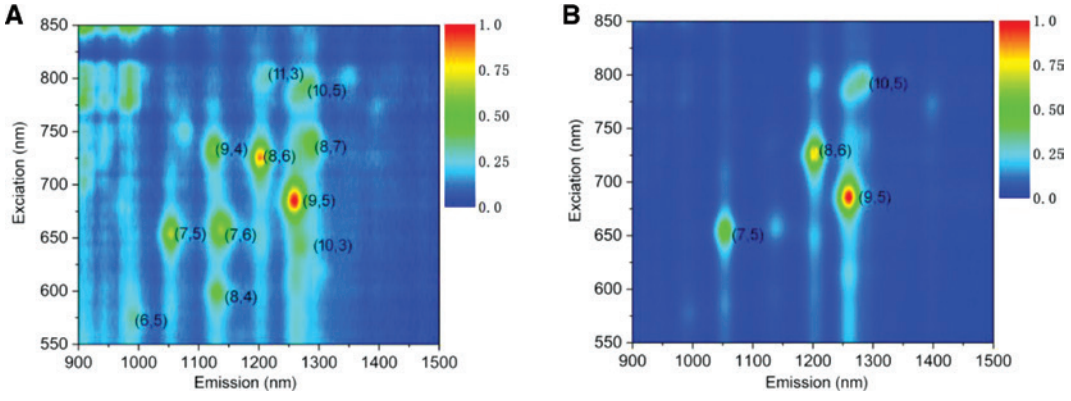

Figure 2: PLE maps of pristine SWCNTs and PFT-sorted s-SWCNTs. (A) Represent the pristine SWCNTs, and (B) represent PFT-sorted s-SWCNTs, respectively.

Table 1: Calibrated contents of the SWCNTs species deduced from the PLE mapping of the PFT-sorted s-SWCNTs.

(n,m)-SWCNTs	Emission peak shift	PL peak intensity	Calculated PL intensity	Calibrated PL peak intensity	Calibrated content
(7,5)-SWCNTs	1054	77,642	0.71	109,355	11.5
(8,6)-SWCNTs	1200	115,264	0.49	235,232	24.8
(9,5)-SWCNTs	1258	141,000	0.28	503,571	53.1
(10,5)-SWCNTs	1270	46,923	0.47	99,836	10.5

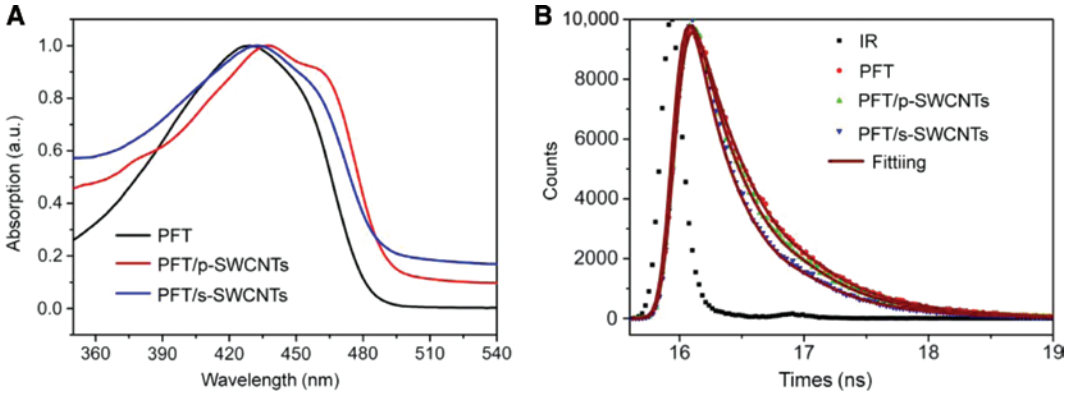

Figure 3: UV-vis absorption spectra and PLE lifetimes. (A) Normalized UV-vis absorption spectra for PFT, PFT/s-SWCNTs, PFT/p-SWCNTs in a toluene solution. (B) PLE lifetimes of PFT polymers in pure PFT, PFT/s-SWCNTs, and PFT/p-SWCNTs in a toluene solution (excitation wavelength at 430 nm, emission wavelength at 505 nm).

The absorption spectrum of PFT exhibited characteristics which conformed with absorption of two of the thiophene (~428 nm) and the fluorene groups (shoulder at ~450 nm). It was worth noting that the absorption peak of PFT in PFT/p-SWCNTs (λ_{max} = 432 nm) and PFT/s-SWCNTs (λ_{max} = 436 nm) toluene solution was red-shifted by ~4 and ~8 nm, respectively. The change was stemmed from the going-up efficient conjugation length within the polymer, by mainly the planarization of polymer backbone and ensuing adsorption upon the SWCNT surface [24, 34]. The larger red-shift of PFT in PFT/s-SWCNTs toluene indicated the larger effective conjugation length of PFT-wrapped s-SWCNTs than the PFT-wrapped pristine SWCNTs which contained one-third of m-SWCNTs.

Time-resolved PLE spectroscopy was applied so as to study transient fluorescence decay of pure PFT, PFT/s-SWCNTs, and PFT/p-SWCNTs solutions in nanosecond timescale (Figure 3B). Each decay curve was well matched by a two-exponential function. The best-matched decay parameters and mean lifetimes are listed in Table 2. The fits of the fluorescence decay for the whole cases realized a desirable fit quality parameter ($\chi^2 < 1.15$) [35] with location around no residuals at random. As per fit results shown in Table 1, the common existence of both slow and fast decays was noticed in all three samples. The pure PFT has a fast component 343 ps (35%) and a slow component 593 ps (65%) with the mean lifetime of 505.5 ps.

Table 2: Two-exponential fitting for the time-resolved PLE spectra of the PFT in different solutions at 505 nm emission wavelength when excited at 430 nm.

	A_1 (%)	τ_1 (ps)	A_2 (%)	τ_2 (ps)	τ_{ave} (ps)
PFT	35%	343	65%	593	505.5
PFT/p-SWCNTs	30%	205	70%	535	436
PFT/s-SWCNTs	48%	166	52%	515	347

A_1 and A_2 are the percentages for the short lifetime τ_1 and long lifetime τ_2, respectively. The average τ_{ave} is calculated using the equation $\tau = A_1\tau_1 + A_2\tau_2$.

The kind of multi-exponential decay was noticed for other polymers because of the existence of multiple chromophore sites of the polymer [36]. After the addition of the acceptor (SWCNTs) to the copolymer solution, the lifetime of the mixture decreased dramatically, which then led to a fast component of 205 ps (30%), a slow component 535 ps (70%) with an average lifetime of 436 ps in the PFT/p-SWCNTs solution, and a fast component of 166 ps (48%) and a slow component 515 ps (52%) with the mean lifetime of 347 ps in the PFT/s-SWCNTs solution. All these results manifested that the decay time (especially in the fast component) for luminescence from PFT-wrapped SWCNT solutions was greatly shortened compared with that of the pure PFT sample. It was speculated that the fast and slow components for luminescence were from PFT in contact

with SWCNTs and not in touch with SWCNTs, respectively, and the fast component indicated the fast energy transfer from PFT to SWCNTs.

Because the fast component of PFT in the PFT/s-SWCNTs toluene solution was obviously shorter than that in the PFT/p-SWCNTs toluene solution, the occurrence of energy transfer was mainly from PFT to s-SWCNTs. Some potential mechanisms come into being for the energy transfer from polymers into s-SWCNTs. Because s-SWCNTs can act as an exciton acceptor, the photoexcitons could be quenched through photoinduced energy transfer channels [37]. As a result, a faster decaying rate for PFT was observed in the PFT/s-SWCNTs toluene solution.

According to the Förster-Dexter theory, excitation energy transfer (EET) was presented when there was a spectral overlap between acceptors and donors, so the determination of energy level alignment can be used to verify whether EET occurs. Figure 5 illustrates the energy levels for PFT and s-SWCNTs. The lowest unoccupied molecular orbital (LUMO) level value is –2.81 eV and the highest occupied molecular orbital (HOMO) level value is –5.34 eV, which were obtained from [38]. The work function of the HiPCO SWCNTs is –4.7 eV [39]. The band edge energies for the valence bands (V_1, V_2, and V_3) and conduction bands (C_1, C_2, and C_3) were derived from the transition energies of E_{11}, E_{22}, and E_{33}. As shown in Figure 4, the C_1 energies of s-SWCNTs are lower than the PFT LUMO level and the V_1 energies of s-SWCNTs are higher than the PFT HOMO level, indicating that there is an overlap between the density of states for the valence and conduction bands of s-SWCNTs and the PFT HOMO and LUMO levels. Such energy level alignment facilitates photoinduced energy transfer from the excited PFT to s-SWCNTs. Moreover, because of the van Hove singularity, a sharp structure appeared in the density of states for SWCNTs at the band edges. When the SWCNT band edges and the PFT energy levels are matched, more efficient EET triggers [32], as well as the occurrence of the chirality chosen as the outcome of the strong interaction between the polymer and specific SWCNTs.

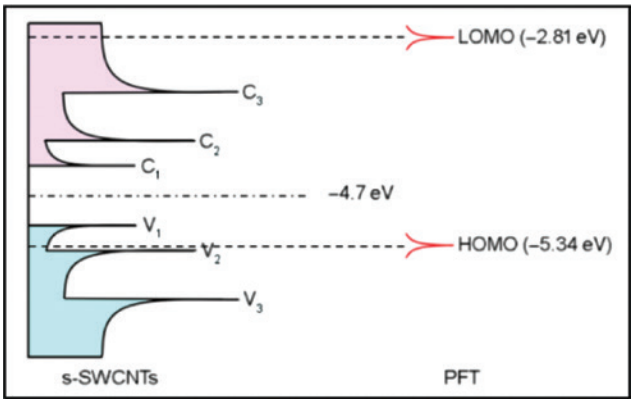

Figure 4: Energy diagram of HOMO and LUMO levels for PFT and s-SWCNTs.

For analyzing the dynamics behavior of photoinduced energy transfer in the PFT-wrapped SWCNTs solution sample, we employed a rate equation model [40]. Within this model the exciton (electron-hole pair) density $n(t)$ in PFT and the exciton density $N(t)$ in SWCNTs are given by

$$dn(t)/dt = g - (\gamma_r + \gamma_{nr} + \gamma_t)n(t) \quad (1)$$

$$dN(t)/dt = G + \gamma_t n(t) - (\Gamma_r + \Gamma_{nr} + \Gamma_t)N(t) \quad (2)$$

where g, γ_r, and γ_{nr} stand for the exciton generation rate, exciton radiative decay rate, and exciton nonradiative decay rate in PFT, respectively. G, Γ_r, and Γ_{nr} stand for the exciton generation rate, exciton radiative decay rate, and exciton nonradiative decay rate in SWCNTs, respectively. γ_t and Γ_t are the energy transfer rate from PFT to SWCNTs and the energy transfer rate from wrapped SWCNT bundles, respectively.

After laser excitation, the exciton density $n(t)$ in Eq. (1) can be written as

$$n(t) = n_o \exp[-(\gamma_r + \gamma_{nr} + \gamma_t)t] \quad (3)$$

Here, n_o stands for the initial exciton density produced by the laser pulse. Eq. (3) suggests that the excitons in PFT are exponentially decaying with the time constant of $(\gamma_r + \gamma_{nr} + \gamma_t)^{-1}$. Thus, combining the time-resolved PLE spectra of the PFT in different solutions, we can compute the value of γ_t. In this study, for the PLE decay of PFT/s-SWCNTs, the average decay constant is 347 ps, so the decay time constant $(\gamma_r + \gamma_{nr} + \gamma_t)^{-1}$ for the exciton density is ~347 ps. The PLE decay time for the pure PFT solution is ~505.5 ps, so $(\gamma_r + \gamma_{nr})^{-1}$ is ~505.5 ps. Thus, the EET rate γ_t was calculated to be $\sim 9 \times 10^8$ s^{-1} by using the calculation of these values. The result suggests that there is energy transfer from PFT to s-SWCNTs in the PFT/s-SWCNTs solution sample. This result is consistent with the previous study in the PFO-wrapped s-SWCNT solution sample by Chen et al. [41]. Using the values in their article, the EET rate γ_t was estimated to be $\sim 7.1 \times 10^8$ s^{-1}, which is close to that in our study. However, due to the influence of thick polymer layers wrapped on the SWCNTs or residual polymers, the EET rates of these solution samples are much smaller than that of the PFO-wrapped SWCNT film sample ($\gamma_t \sim 2.6 \times 10^{12}$ s^{-1}) [40]. Thus, in order to improve

the energy transfer efficiency, the ratio of s-SWCNTs in the PFT-wrapped s-SWCNT resultant hybrids should be further enhanced.

3.3 MD simulations

MD simulation is an important computer simulation method to study molecular systems at atomic level [42, 43]. In this work, MD simulation was performed for a better understanding of the interaction between PFT and different SWCNT species. At first, the binding energy between PFT and (9,5)-, (8,6)-, (7,5)-, and (10,5)-SWCNTs was calculated as they were selectively extracted by PFT in the experiment. Then, the binding energy between PFT and (7,6)-, (9,4)-SWCNTs, which were plenty in the unsorted SWCNTs but almost disappeared in the PFT-sorted SWCNTs, was also calculated. The binding energy, $E_{binding}$, was identified as the non-bond energy (van der Waals and Columbic) between PFT and SWCNTs. It was calculated according to the following equation [44]:

$$E_{binding} = E_{total} - (E_{PFT} + E_{SWCNTs}) \quad (4)$$

where E_{total}, E_{PFT}, and E_{SWCNTs} stand for the total non-bond energy of the composite, the non-bond energy of the PFT without the nanotube, and the non-bond energy of the nanotube without PFT wrapping in the final equilibrated structures, respectively. In other words, the binding energy can be calculated as the difference between the energy of the optimized composite structure and the energy of an infinitely separated nanotube and polymer. The starting configuration and results of MD simulation targeting different PFT-SWCNT combinations are shown in Figure 5.

As shown in Figure 5, the PFTs were well wrapped around (9,5)-, (8,6)-, (7,5)-, (10,5)-, (7,6)-, and (9,4)-SWCNTs, endowing the SWCNTs' good dispersibility. The MD simulation indicated that PFT with the (9,5)-SWCNT system had the lowest binding energy, which meant that the PFT had the highest preference or selectivity toward (9,5)-SWCNTs. This is in good agreement with the experimental results. Since (9,5)-SWCNTs can provide a potential energy surface, which made the PFT take its favorite conformational structure and show the most likely twist angle, the π-π interaction between the conjugated units in the PFT and SWCNTs was enhanced [45] and thus led to selective enrichment via PFT solution extraction. In contrast, the binding energy of PFT with (7,6)- and (9,4)-SWCNTs was much weaker; as a result, (7,6)- and (9,4)-SWCNTs almost vanish after PFT solution extraction although they are plenty in the starting materials. The binding energy between PFT

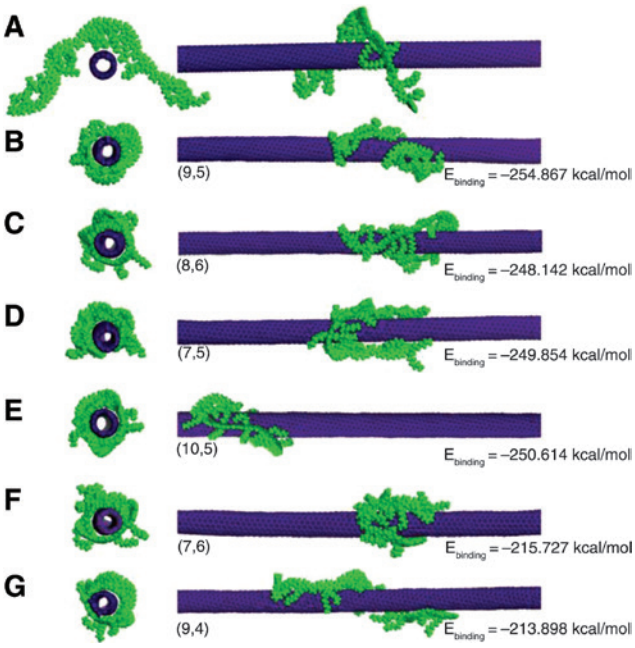

Figure 5: The cross-sectional and the horizontal views of the wrapping configurations of PFT on SWCNTs with different chiralities. (A) Schematics of the starting structure to perform MD simulations, (B) PFT-(9,5)-SWCNTs, (C) PFT-(8,6)-SWCNTs, (D) PFT-(7,5)-SWCNTs, (E) PFT-(10,5)-SWCNTs, (F) PFT-(7,6)-SWCNTs, and (G) PFT-(9,4)-SWCNTs.

and (8,6)-, (10,5)-, (7,5)-SWCNTs is very close and slightly lower than that between PFT and (9,5)-SWCNTs but much larger than that between PFT and (7,6)- and (9,4)-SWCNTs. Consequently, (8,6)-, (10,5)-, (7,5)-SWCNTs are relatively enriched after PFT solution extraction. In brief, the MD simulations are in good agreement with the experimental results. Although more sophisticated simulations, such as the effects of electronic structures and charges, need to be carried out to fully understand the PFT sorting mechanism, the current research provided an insight into the interactions between PFT and SWCNTs.

4 Conclusions

A fluorene and thiophene containing conjugated polymers (PFT) were synthesized to investigate their interaction with SWCNTs. The UV-vis-NIR, Raman, and PLE spectra indicated that the PFT had high selectivity toward specific chirality of s-SWCNTs. The amount ratios of the sorted s-SWCNTs with chiralities of (n,m) = (9,5), (8,6), (7,5), and (10,5) were 53.1%, 24.8%, 11.5%, and 10.5%, respectively. Both steady-state and transient optical spectra of PFT confirmed the strong interaction between PFT and s-SWCNTs. Moreover, when the energy levels of the polymer

and s-SWCNTs match well, strong electrical interactions between the polymer and s-SWCNTs can occur. In addition, the analyzing results of the photoinduced energy transfer behavior of the PFT-wrapped s-SWCNT resultant hybrids showed that the energy transfer efficiency was affected by the ratio of s-SWCNTs. The MD simulation results indicated that the polymers were capable of surrounding SWCNTs and showed chosen interactions with the s-SWCNT categories. Therefore, the strong interaction between polymer and s-SWCNTs can be used to enrich s-SWCNTs and enhance the performance of the devices they applied.

Acknowledgments: This research was generously supported by the Natural Science Foundation of China (Nos. 60970815 and 61275179), the Natural Science Basic Research Plan in Shaanxi Province of China (Program No. 2016JM8047), the Fundamental Funds for the Central Universities (No. xjj2015112), ShaanXi Province Administration of Traditional Chinese Medicine (15-ZY036), and Xi'an Medical University state fund cultivation project (2016GJF01).

References

[1] Shulaker MM, Hills G, Patil N, Wei H, Chen H, Wong HSP, Mitra S. Carbon nanotube computer. *Nature* 2013, 501, 526–530.
[2] Javey A, Wang Q, Lundstrom M, Dai H, Guo J. Ballistic carbon nanotube field-effect transistors. *Nature* 2003, 424, 654–657.
[3] Arnold MS, Green AA, Hulvat JF, Stupp SI, Hersam MC. Sorting carbon nanotubes by electronic structure using density differentiation. *Nat. Nanotech.* 2006, 1, 60–65.
[4] Zheng M, Jagota A, Strano MS, Santos AP, Barone P, Chou SG, Diner BA, Dresselhaus MS, McLean RS, Onoa GB, Samsonidze GG, Semke ED, Usrey M, Walls DJ. Structure-based carbon nanotube sorting by sequence-dependent DNA assembly. *Science* 2003, 302, 1545–1548.
[5] Nish A, Hwang JY, Doig J, Nicholas RJ. Highly selective dispersion of single-walled carbon nanotubes using aromatic polymers. *Nat. Nanotech.* 2007, 2, 640–646.
[6] Lei T, Pitner G, Chen X, Hong G, Park S, Hayoz P, Weitz RT, Wong HP, Bao Z. Dispersion of high-purity semiconducting arc-discharged carbon nanotubes using backbone engineered diketopyrrolopyrrole (DPP)-based polymers. *Adv. Electron Mater.* 2016, 2, 1500299.
[7] Park S, Lee HW, Wang H, Selvarasah S, Dokmeci MR, Park YJ, Cha SN, Kim JM, Bao Z. Highly effective separation of semiconducting carbon nanotubes verified via short-channel devices fabricated using dip-pen nanolithography. *ACS Nano* 2012, 6, 2487–2496.
[8] Salazar-Rios JM, Gomulya W, Derenskyi V, Yang J, Bisri SZ, Chen Z, Facchetti A, Loi MA. Selecting semiconducting single-walled carbon nanotubes with narrow bandgap naphthalene diimide-based polymers. *Adv. Electron Mater.* 2015, 1, 1500074.
[9] Wang H, Mei J, Liu P, Schmidt K, Jiménez-Osés G, Osuna S, Fang L, Tassone CJ, Zoombelt AP, Sokolov AN, Houk KN, Toney MF, Bao Z. Scalable and selective dispersion of semiconducting arc-discharged carbon nanotubes by dithiafulvalene/thiophene copolymers for thin film transistors. *ACS Nano* 2013, 7, 2659–2668.
[10] Lee HW, Yoon Y, Park S, Oh JH, Hong S, Liyanage LS, Wang H, Morishita S, Patil N, Park YJ, Park JJ, Spakowitz A, Galli G, Gygi F, Wong PHS, Tok JBH, Kim JM, Bao Z. Selective dispersion of high purity semiconducting single-walled carbon nanotubes with regioregular poly(3-alkylthiophene)s. *Nat. Commun.* 2011, 2, 541.
[11] Mallajosyula AT, Nie W, Gupta G, Blackburn JL, Doorn SK, Mohite AD. Critical role of the sorting polymer in carbon nanotube-based minority carrier devices. *ACS Nano* 2016, 10, 10808–10815.
[12] Arici E, Karazhanov S. Carbon nanotubes for organic/inorganic hybrid solar cells. *Mat. Sci. Semicon. Proc.* 2016, 41, 137–49.
[13] Wang H, Koleilat GI, Liu P, Jiménez-Osés G, Lai Y, Vosgueritchian M, Fang Y, Park S, Houk KN, Bao Z. High-yield sorting of small-diameter carbon nanotubes for solar cells and transistors. *Acs Nano* 2014, 8, 2609–2617.
[14] Han J, Ji Q, Qiu S, Li H, Zhang S, Jin H, Li Q. A versatile approach to obtain a high-purity semiconducting single-walled carbon nanotube dispersion with conjugated polymers. *Chem. Commun.* 2015, 51, 4712–4714.
[15] Lee S, Kim D, Noh Y. Improved ambipolar charge injection in organic field-effect transistors with low cost metal electrode using polymer sorted semiconducting carbon nanotubes. *Org. Electron.* 2017, 46, 28–34.
[16] Wang C, Qian L, Xu W, Nie S, Gu W, Zhang J, Zhao J, Lin J, Chen Z, Cui Z. High performance thin film transistors based on regioregular poly(3-dodecylthiophene)-sorted large diameter semiconducting single-walled carbon nanotubes. *Nanoscale* 2013, 5, 4156.
[17] Gu J, Han J, Liu D, Yu X, Kang L, Qiu S, Jin H, Li H, Li Q, Zhang J, Solution-processable high-purity semiconducting SWCNTs for large-area fabrication of high-performance thin-film transistors. *Small* 2016, 12, 4993–4999.
[18] Lemasson FA, Strunk T, Gerstel P, Hennrich F, Lebedkin S, Barner-Kowollik C, Wenzel W, Kappes MM, Mayor M. Selective dispersion of single-walled carbon nanotubes with specific chiral indices by poly(N-decyl-2,7-carbazole). *J. Am. Chem. Soc.* 2011, 133, 652–655.
[19] Gao J, Kwak M, Wildeman J, Herrmann A, Loi MA. Effectiveness of sorting single-walled carbon nanotubes by diameter using polyfluorene derivatives. *Carbon* 2011, 49, 333–338.
[20] Bottacchi F, Petti L, Späth F, Namal I, Tröster G, Hertel T, Anthopoulos TD. Polymer-sorted (6,5) single-walled carbon nanotubes for solution-processed low-voltage flexible microelectronics. *Appl. Phys. Lett.* 2015, 106, 193302.
[21] Tange M, Okazaki T, Iijima S. Selective extraction of large-diameter single-wall carbon nanotubes with specific chiral indices by poly(9,9-dioctylfluorene-alt-benzothiadiazole). *J. Am. Chem. Soc.* 2011, 133, 11908–11911.
[22] Liu B, Yu W, Lai Y, Huang W. Synthesis, Characterization, and structure–property relationship of novel fluorene–thiophene-based conjugated copolymers. *Macromolecules* 2000, 33, 8945–8952.

[23] Liu Z, Li H, Qiu Z, Zhang S, Zhang Z. Small-hysteresis thin-film transistors achieved by facile dip-coating of nanotube/polymer composite. *Adv. Mater.* 2012, 24, 3633–3638.
[24] Qian L, Xu W, Fan X, Wang C, Zhang J, Zhao J, Cui Z. Electrical and photoresponse properties of printed thin-film transistors based on poly(9,9-dioctylfluorene-co-bithiophene) sorted large-diameter semiconducting carbon nanotubes. *J. Phys. Chem. C* 2013, 117, 18243–18250.
[25] Xu W, Zhao J, Qian L, Han X, Wu L, Wu W, Song M, Zhou L, Su W, Wang C, Nie S, Cui Z. Sorting of large-diameter semiconducting carbon nanotube and printed flexible driving circuit for organic light emitting diode (OLED). *Nanoscale* 2014, 6, 1589–1595.
[26] Chen N, Lu J, Wang D, Zheng C, Wu H, Zhang H, Gao D. A double-cable poly(fluorene-alt-thiophene) with bay-substituted perylenediimide pendants: an efficient interfacial material in bulk-heterojunction solar cells. *Macromolecules* 2017, 51, 80–90.
[27] Lebedkin S, Arnold K, Kiowski O, Hennrich F, Kappes MM. Raman study of individually dispersed single-walled carbon nanotubes under pressure. *Phys. Rev. B* 2006, 73, 094109.
[28] Cao Q, Han S, Tulevski GS, Zhu Y, Lu DD, Haensch W. Arrays of single-walled carbon nanotubes with full surface coverage for high-performance electronics. *Nat. Nanotech.* 2013, 8, 180–186.
[29] Yi W, Malkovskiy A, Chu Q, Sokolov AP, Colon ML, Meador M, Pang Y. Wrapping of single-walled carbon nanotubes by a π-conjugated polymer: the role of polymer conformation-controlled size selectivity. *J. Phys. Chem. B* 2008, 112, 12263–12269.
[30] Fukumaru T, Toshimitsu F, Fujigaya T, Nakashima N. Effects of the chemical structure of polyfluorene on selective extraction of semiconducting single-walled carbon nanotubes. *Nanoscale* 2014, 6, 5879.
[31] Bachilo SM, Strano MS, Kittrell C, Hauge RH, Smalley RE, Weisman RB. Structure-assigned optical spectra of single-walled carbon nanotubes. *Science* 2002, 298, 2361–2366.
[32] Weisman RB, Bachilo SM. Dependence of optical transition energies on structure for single-walled carbon nanotubes in aqueous suspension: an empirical kataura plot. *Nano Lett.* 2003, 3, 1235–1238.
[33] Oyama Y, Saito R, Sato K, Jiang J, Samsonidze GG, Grüneis A, Miyauchi Y, Maruyama S, Joriod A, Dresselhaus G, Dresselhause MS. Photoluminescence intensity of single-wall carbon nanotubes. *Carbon* 2006, 44, 873–879.
[34] Yi W, Malkovskiy A, Xu Y, Wang X, Sokolov AP, Lebron-Colon M, Meador MA, Pang Y. Polymer conformation-assisted wrapping of single-walled carbon nanotube: the impact of cis-vinylene linkage. *Polymer* 2010, 51, 475–481.
[35] Nguyen V, Si J, Yan L, Hou X. Electron–hole recombination dynamics in carbon nanodots. *Carbon* 2015, 95, 659–663.
[36] Taya P, Maiti B, Kumar V, De P, Satapathi S. Design of a novel FRET based fluorescent chemosensor and their application for highly sensitive detection of nitroaromatics. Sens. *Actuators B Chem.* 2018, 255, 2628–2634.
[37] Yi W, Yoo S, Wang S, Kong J, Si J, Gong Q, Hou X, Dresselhaus MS. The nano necklace made of single-walled carbon nanotubes and an azo-containing polymer: Island-like carboxyl distribution, bead-like morphology formation, and photophysical properties manipulation. *Carbon* 2016, 108, 112–119.
[38] Barbosa CG, Bento DC, Péres LO, Louarn G, de Santana H. Changes induced by electrochemical oxidation of poly(9,9-dioctylfluorene-alt-thiophene): towards a correlation between charge transport, molecular structure modifications and degradation. *J. Mater. Sci. Mater. Electron.* 2016, 27, 10259–10269.
[39] Suzuki S, Watanabe Y, Homma Y, Fukuba S, Heun S, Locatelli A. Work functions of individual single-walled carbon nanotubes. *Appl. Phys. Lett.* 2004, 85, 127–129.
[40] Nakamura A, Koyama T, Miyata Y, Shinohara H. Ultrafast energy transfer from fluorene polymers to single-walled carbon nanotubes in wrapped carbon nanotube bundles. *J. Phys. Chem. C* 2016, 120, 4647–4652.
[41] Chen F, Zhang W, Jia M, Wei L, Fan X, Kuo J, Chen Y, Chan-Park MB, Xia A, Li L. Energy transfer from photo-excited fluorene polymers to single-walled carbon nanotubes. *J. Phys. Chem. C* 2009, 113, 14946–14952.
[42] Vijayaraghavan V, Dethan JFN, Garg A. Nanomechanics and modelling of hydrogen stored carbon nanotubes under compression for PEM fuel cell applications. *Comp. Mater. Sci.* 2018, 146, 176–183.
[43] Vijayaraghavan V, Zhang L. Effective mechanical properties and thickness determination of boron nitride nanosheets using molecular dynamics simulation. *Nanomaterials-Basel* 2018, 8, 546.
[44] Zhou C, Zhao J, Ye J, Tange M, Zhang X, Xu W, Zhang K, Okazaki T, Cui Z. Printed thin-film transistors and NO_2 gas sensors based on sorted semiconducting carbon nanotubes by isoindigo-based copolymer. *Carbon* 2016, 108, 372–380.
[45] Xu W, Dou J, Zhao J, Tan H, Ye J, Tange M, Gao W, Xu W, Zhang X, Guo W, Ma C, Okazaki T, Zhang K, Cui Z. Printed thin film transistors and CMOS inverters based on semiconducting carbon nanotube ink purified by a nonlinear conjugated copolymer. *Nanoscale* 2016, 8, 4588–4598.